Theor Chem Acc (2009) 124:105–113
DOI 10.1007/s00214-009-0587-z

REGULAR ARTICLE

Mechanistic and dual-level direct dynamics studies on the reaction Cl + CH_2FCl

Xiu-Juan Jia · You-Jun Liu · Jing-Yu Sun · Yi-Zhen Tang · Hao Sun · Li-Zhu Hao · Rong-Shun Wang · Xiu-Mei Pan

Received: 1 January 2009 / Accepted: 12 May 2009 / Published online: 29 May 2009

Abstract Theoretical investigations are carried out on the reaction Cl + CH_2FCl by means of direct dynamics method. The minimum energy path (MEP) is obtained at the MP2/6-311G(d, p) level. The energetic information is further improved by single-point energy calculations using QCISD(T)/6-311++G(d, p) method. The kinetics of this reaction are calculated by canonical variational transition state theory incorporating with the small-curvature tunneling correction over a wide temperature range of 220–3,000 K, and rate constant expression are found to be $k(T) = 1.48 \times 10^{-17} T^{2.04} \exp(-913.91/T)$. For the title reaction, H-abstraction reaction channel is the major channel at the lower temperatures. At higher temperatures, the contribution of Cl-abstraction reaction channel should be taken into account.

X.-J. Jia · J.-Y. Sun · Y.-Z. Tang · H. Sun · R.-S. Wang (✉) · X.-M. Pan (✉)
Faculty of Chemistry, Institute of Functional Material Chemistry, Northeast Normal University, 130024 Changchun, People's Republic of China
e-mail: wangrs@nenu.edu.cn

X.-M. Pan
e-mail: panxm460@nenu.edu.cn

X.-J. Jia
e-mail: jiaxj753@nenu.edu.cn

Y.-J. Liu
Faculty of Physics, Aviation University of Air Force, 130022 Changchun, People's Republic of China

L.-Z. Hao
Key Laboratory for Applied Statistics of MOE (KLAS), School of Mathematics and Statistics, Northeast Normal University, 130024 Changchun, Jilin, People's Republic of China

Keywords Dual level dynamics · Cl + CH_2FCl · Minimum energy path (MEP)

1 Introduction

The importance of haloalkanes in atmospheric chemistry is well established [1–5]. Chlorine atom chemistry is of great importance over a wide temperature range. At low temperatures (200–300 K), Chlorine atom plays an active role as ozone destroyer in the atmosphere, and it is important for combustion chemistry at high temperatures (1,000–2,500 K). Hydrochlorofluorocarbons (HCFCs) are emitted into the atmosphere from a number of sources. HCFCs contain Cl atoms and thus contribute to ozone depletion. Chlorine atom reactions play a role in the destruction of these species in the stratosphere [6]. Halogen-substituted hydrocarbons, attacked by Cl atom in the gas phase, also play an important role in the process of industrial chlorination and in the incineration of hazardous halogenated wastes [7]. Experimentally and theoretically, the mechanism and kinetics of such reactions of haloalkanes with various free radicals have been extensively studied and continue to receive considerable attention [8–15].

CH_2FCl is a classical species of halogen-substituted hydrocarbons, and its reaction with Cl atoms can proceed via three reaction channels, e.g.

$$Cl + CH_2FCl \rightarrow CHFCl + HCl \quad (R1)$$

$$Cl + CH_2FCl \rightarrow CH_2F + Cl_2 \quad (R2)$$

$$Cl + CH_2FCl \rightarrow CH_2Cl + ClF \quad (R3)$$

There are some experimental studies concerning rate constants for the title reaction [16–21]. In 1988, Tschuikow-Roux and co-workers [16] reported the H-abstraction

channel of the title reaction by using the competitive method with methane as a primary standard, and the experimental rate constant was obtained as $(1.91 \pm 0.57) \times 10^{-13}$ cm^3/(molecule s) at 298 K. In 1992, Tuazon et al. [18] studied the rate constant of the title reaction by means of a relative rate technique, and the experimental rate constant was determined as $(1.1 \pm 0.25) \times 10^{-13}$ cm^3/(molecule s) at 298 K. The other experimental rate constant of the reaction $CH_2FCl + Cl \rightarrow HCl + CHFCl$ was determined as $1.0 \times 10^{-11}e^{[-11.141 \pm 4.124]/RT}$ [in cm^3/(molecule s)] given by Atkinson and co-workers in the temperature region of 273–368 K [21]. The temperature used in the experiment does not cover the whole temperature range of practical interest; therefore, the accurate extrapolation of rate constants to higher temperatures requires the theoretical study. Because no experimental information is available on the branching ratio of the rate constants of the title reaction, theoretical investigation is desirable to give a further understanding of the reaction mechanism and the dynamics property of the multiple channel reaction $Cl + CH_2FCl$. To our best knowledge, no previous theoretical work has addressed this reaction.

In this paper, the mechanism of Cl reaction with CH_2FCl is investigated and dual-level direct dynamics studies [22–26] are carried out on this reaction to obtain the rate constants over a wide temperature region of 220–3,000 K. The potential energy surface information, including geometries, energies, gradients, and force constants of the stationary points (reactants, products, complexes and transition states) and extra points along the minimum energy path (MEP), is obtained directly from electronic structure calculations. Subsequently, the rate constants are calculated by the variational transition state theory (VTST) proposed by Truhlar and co-workers [27, 28]. The comparison between theoretical and experimental results has been discussed.

2 Computational methods

All the electronic structure calculations were carried out with Gaussian 03 program package [29]. The equilibrium geometries and frequencies of the reactant, products, complexes and transition states are optimized at the restricted or unrestricted second-order perturbation Møller-Plesset level of theory (MP2) [30] using the standard 6-311G(d, p) basis set. At the same level, the MEP is obtained by intrinsic reaction coordinate (IRC) theory in mass-weighted Cartesian coordinates with a gradient step-size 0.05 $(amu)^{1/2}$ bohr. Furthermore, the energy profile is refined at the QCISD(T)/6-311++G(d, p) [31] level based on the MP2/6-311G(d, p) geometries. The force constant matrices of the stationary points and selected nonstationary points near the transition state along the MEP have been also calculated in order to do the following kinetics calculations.

By means of the POLYRATE 9.1 program [32], the dynamics calculations are performed by using the variational transition-state theory (VTST) [27, 28] with the interpolated single-point energies (ISPE) method [33]. The ISPE method is a dual-level direct dynamics scheme that uses a low-level MEP and corrects the energy by interpolating the energy differences at some points along this low-level MEP and single-point energy calculations at a higher-level. The specific form of VTST that we used is canonical variational transition-state theory (CVT) [34–37] with the small-curvature tunneling (SCT) [38, 39] contributions proposed by Truhlar and co-workers. In the calculation of the reactant electronic partition function, two electronic states of Cl atoms, $^2P_{1/2}$ and $^2P_{3/2}$, are included, with an 881 cm^{-1} splitting due to spin–obit coupling. All of the vibrational modes were treated as quantum-mechanical separable harmonic oscillators. During the kinetic calculations, the Euler single-step integrator with a step size of 0.0001 $(amu)^{1/2}$ bohr is adopted to follow the MEP, and the generalized normal-mode analysis is performed every 0.01 $(amu)^{1/2}$ bohr. The curvature components are calculated using a quadratic fit to obtain the derivative of the gradient with respect to the reaction coordinate.

3 Results and discussion

3.1 The stationary points

The optimized geometric parameters of the reactant (CH_2FCl), products (CHFCl, HCl, CH_2F, Cl_2, CH_2Cl, and ClF), complexes (CP_{R1}, CP_{R2}, CR_{R3}) and transition states (TS1, TS2, and TS3) for three reaction channels, reaction R1, reaction R2, and reaction R3, calculated at the MP2/6-311G(d, p) level along with the available experimental data [40–42] are presented in Fig. 1. From Fig. 1, we can see that the largest deviation between the theoretical bond lengths and the experimental values is 0.041 Å (r (Cl–Cl) for Cl_2) and the largest deviation of the bond angles is 4.8° for $\angle H_1CCl$ in CH_2Cl. It is obvious that the theoretical geometric parameters are in good agreement with the experimental data. Furthermore, there are two product complexes (CP_{R1}, CP_{R2}) on the products sides for R1 and R2, and one reactant complex (CR_{R3}) on reactant side in reaction R3. Good agreement between the theoretical and experimental values of CH_2FCl, CH_2Cl, HCl, and Cl_2 might imply that the same accuracy could be expected for the calculated geometries of complexes and transition states. At the MP2/6-311G(d, p) level, the C···H bond

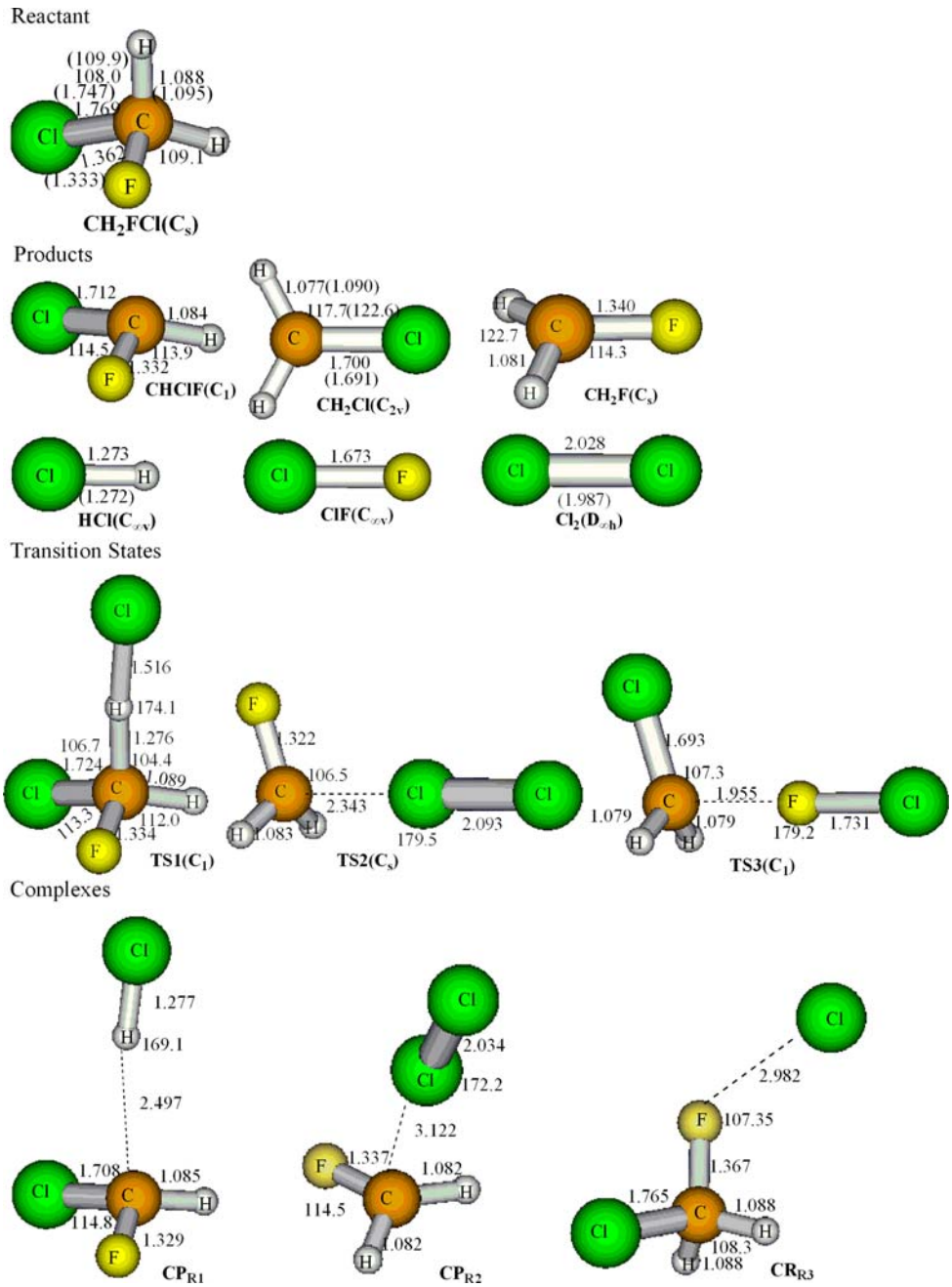

Fig. 1 Optimized geometries of the reactant, products, complexes and transition states at the MP2/6-311G(d, p) level. The values in parentheses are the experimental values (Ref. [40] for CH_2Cl, Ref. [41] for HCl and Cl_2, Ref. [42] for CH_2FCl). Bond lengths are in angstroms, and angles are in degrees

distance in CP_{R1} is 2.497 Å, while the other bond lengths are very close to those of the products. CP_{R1} is a weakly hydrogen-bonded complex between the HCl molecule and the CHFCl radical. The hydrogen bonding occurs between the hydrogen atom of HCl and the methylidyne carbon of CHFCl. The transition states TS1 for reaction R1 and TS3 for reaction R3 have the same symmetry, i.e., C_1 symmetry. For reaction R2, the transition state TS2 has C_s symmetry. In the transition state structure TS1, the breaking C–H bond stretches by 18% over the C–H regular bond length in CH_2FCl, and the product-forming H–Cl bond is elongated by about 24% compared with the equilibrium bond length in isolated HCl. Thus, reaction R1 proceeds via early barrier. In the structure of TS2 and TS3, the C–Cl and C–F bonds that will be broken, increase by 57 and 59% compared with the C–Cl and C–F equilibrium bond lengths in CH_2FCl, and the forming Cl–Cl and F–Cl bonds are about 6 and 5% longer than the regular bond length of the isolated Cl_2 and ClF, respectively. This implies that the two transition states are both near the corresponding products, and these two reactions will both proceed via late transition states.

Table 1 gives the harmonic vibrational frequencies of the reactant, products, complexes, and transition states at

Table 1 Calculated and experimental frequencies (cm^{-1}) for the reactant, products, complexes and transition states for the title reaction at the MP2/6-311G(d, p) level

Species	MP2/6-311G(d, p)	Expt
CH_2FCl	398, 799, 1,043, 1,120, 1,296, 1,439, 1,526, 3,147, 3,229	385[a], 760[a], 1,001[a], 1,068[a], 1,236[a], 1,351[a], 1,468[a], 2,993[a], 3,048[a]
CHClF	419, 804, 899, 1,199, 1,361, 3,242	410[b], 757[b], 910[b], 1,250[b]
HCl	3,090	2,991[a]
CH_2F	713, 1,205, 1,212, 1,519, 3,195, 3,353	1,163[b], 1,170[b], 3,044[b], 318[b]
Cl_2	539	549[c]
CH_2Cl	277, 877, 1,048, 1,473, 3,236, 3,390	389[b], 829[b], 1,391[b], 3,055[b]
ClF	734	
CP_{R1}	19, 35, 64, 208, 216, 422, 819, 904, 1,205, 1,361, 3,031, 3,237	
CP_{R2}	17, 39, 55, 95, 153, 539, 744, 1,212, 1,213, 1,519, 3,192, 3,352	
CR_{R3}	3, 63, 74, 398, 803, 1,043, 1,104, 1,297, 1,440, 1,524, 3,153, 3,235	
TS1	1204*i*, 91, 163, 374, 453, 862, 989, 1,092, 1,180, 1,257, 1,377, 3,184	
TS2	1,309*i*, 76, 129, 211, 498, 564, 868, 933, 1,073, 1,483, 3,232, 3,377	
TS3	443*i*, 69, 85, 191, 416, 522, 1,005, 1,229, 1,229, 1,519, 3,185, 3,341	

[a] Ref. [43]

[b] Ref. [44]

[c] Ref. [45]

Table 2 Reaction enthalpies ($\Delta H°_{298}$), the relative energies with ZPE correction of complexes (ΔE^c) and potential barrier of the transition states (ΔE^{TS}) (kcal/mol), classical barrier height (V_{MEP}), vibrationally adiabatic barrier height (V_a^G) for the three reactions and together with the experimental values

		MP2/6-311G (d, p)	QCISD(T)/6-311++ G(d, p)//MP2/6-311G(d, p)	Expt[a]
$CH_2FCl + Cl \rightarrow CHFCl + HCl$	$\Delta H°_{298}$	−4.83	−1.13	−3.0 ± 2.4
	ΔE^{TS} + ZPE	5.02	3.64	
CP_{R1}	ΔE^c + ZPE	−2.26	−2.73	
	V_{MEP}	9.27	7.89	
	V_a^G	25.04	23.65	
$CH_2FCl + Cl \rightarrow CH_2F + Cl_2$	$\Delta H°_{298}$	37.85	37.29	
	ΔE^{TS} + ZPE	43.39	37.73	
CP_{R2}	ΔE^c + ZPE	39.20	35.90	
	V_{MEP}	45.12	39.45	
	V_a^G	63.41	57.74	
$CH_2FCl + Cl \rightarrow CH_2Cl + ClF$	$\Delta H°_{298}$	55.89	55.45	49.9 ± 2.0
	ΔE^{TS} + ZPE	76.29	62.89	
CR_{R3}	ΔE^c + ZPE	−1.30	−1.96	
	V_{MEP}	78.52	65.11	
	V_a^G	96.31	82.90	

[a] Experimental value derived from the standard heats of formation (in kcal/mol): [46] for CH_2FCl (−62.6 kcal/mol); HCl (−22.1 kcal/mol); Cl (29.0 kcal/mol); ClF (−12.0 kcal/mol); [47] for CHFCl (14.51 ± 2.4 kcal/mol) [48] for CH_2Cl (28.3 ± 2.0 kcal/mol)

the MP2/6-311G(d, p) level as well as the corresponding experimental results [43–45]. For the species of reactant and products, the calculated frequencies are in good agreement with the experimental values, for each transition state yields one and only one imaginary frequency corresponding to the stretching modes of the coupling breaking and forming bonds. The values of those imaginary frequencies are 1204.0*i*, 1309.3*i*, and 443.5*i* cm^{-1} for reaction R1, R2, and R3, respectively.

The reaction enthalpies ($\Delta H°_{298}$), the relative energies of hydrogen-bonded complexes (ΔE^c), and the potential barrier of the transition states (ΔE^{TS}) (kcal/mol) with zero-point (ZPE) corrections for reactions R1, R2, and R3 calculated at the MP2/6-311G(d, p) level and QCISD(T)/6-311++G(d, p)//MP2/6-311G(d, p) level are listed in Table 2, as well as the available experimental reaction enthalpies [46–48]. The theoretical values at 298 K of $\Delta H°_{298}$, −1.13 and 55.45 kcal/mol for reactions R1 and R3 are in reasonable agreement with the corresponding experimental values, −3.0 ± 2.4 and 49.9 ± 2.0 kcal/mol.

The profile of potential energy surface of the title reaction obtained at the QCISD(T)/6-311 ++G(d, p)// MP2/6-311G(d, p)+ZPE level is described in Fig. 2. Note

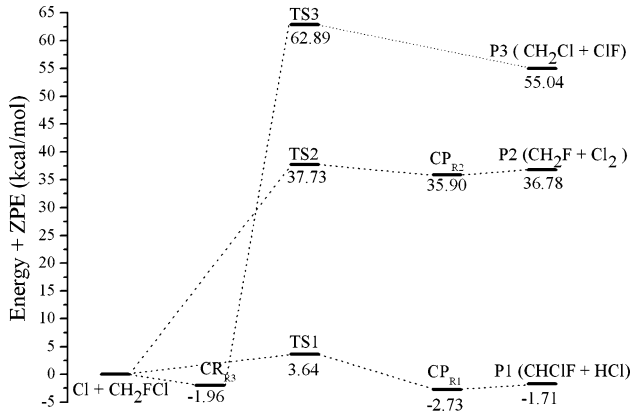

Fig. 2 Schematic potential energy surface for the title reaction. Relative energies (in kcal/mol) are calculated at the QCISD(T)/6-311++G(d, p)//MP2/6-311G(d, p) + ZPE level

that the energies of reactants are set to be zero for reference. For reaction R1, the attack of Cl atom on the C–H bond of CH_2FCl would proceed via a hydrogen-bonded complex (CP_{R1}) on the product side, which is 2.73 kcal/mol lower than the reactants. For reaction R2 and R3, the product complex (CP_{R2}) and reactant complex (CR_{R3}) are located at the exit and the entrance of the channels, respectively, and so they proceed via indirect mechanisms. The energy of complex CP_{R2} is 35.90 kcal/mol higher than that of reactants, and the energy of complex CR_{R3} is 1.96 kcal/mol lower than that of reactants. The barrier heights of reactions R2 and R3 are 34.09 and 59.25 kcal/mol higher than that of reaction R1 (3.64 kcal/mol). Thus, the H-abstraction channel is more favorable, and the halogen abstraction channels are minor pathway. At the same time, the H-abstraction reaction R1 is exothermic by 1.71 kcal/mol, while reaction R2 and R3 are endothermic by 36.78 and 55.04 kcal/mol, respectively, which indicates that reaction R1 is thermodynamically more favorable than reactions R2 and R3, and the rate constants of reaction R1 will be larger than those of the other two reactions (R2 and R3). This view will be further testified in the following study of the rate constants.

3.2 Minimum energy path

The changes of bond lengths along the IRC for the Cl reaction with CH_2FCl are plotted in Fig. 3. From Fig. 3a, it is easily seen that with the proceeding of the H– abstraction reaction channel, the breaking C–H bond and forming H–Cl bond lengths change smoothly up to the about $s = -0.45$ $(amu)^{1/2}$ bohr. After that, both bonds change

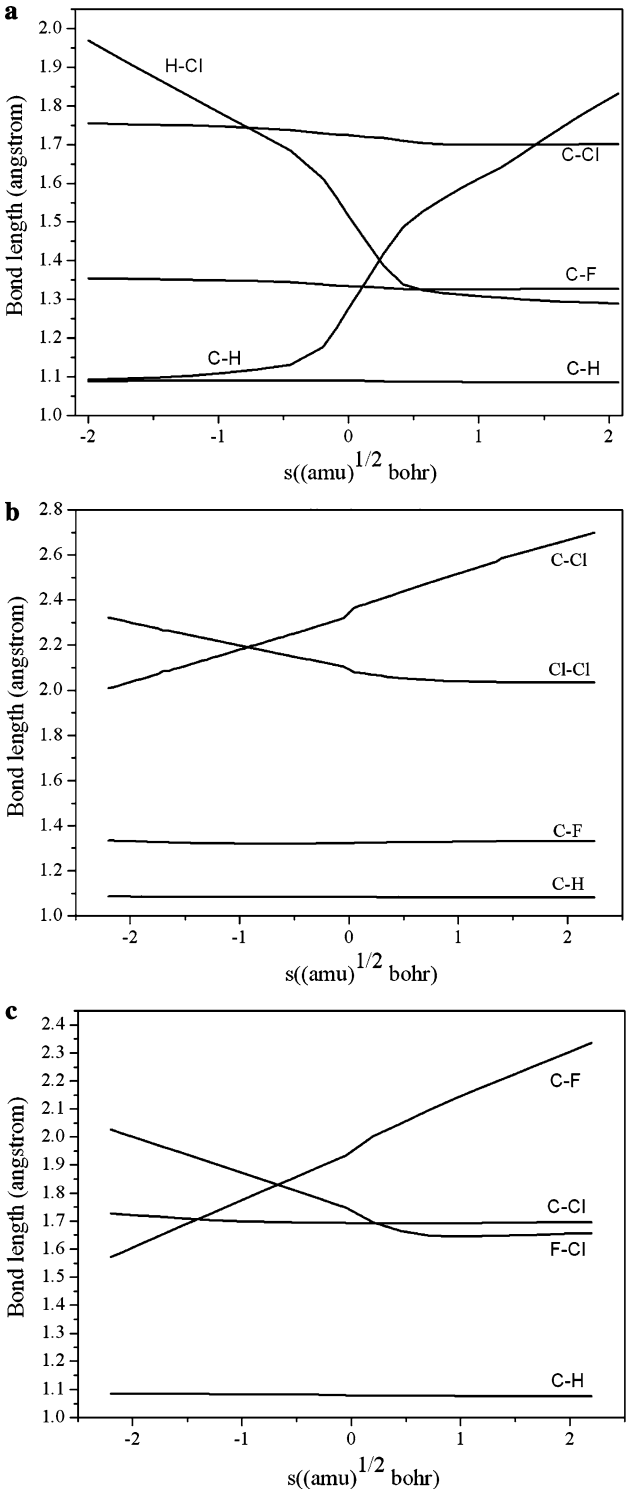

Fig. 3 **a** Changes of the bond lengths along the MP2/6-311G(d, p) minimum energy path for the Cl + CH_2FCl → CHFCl + HCl. **b** Same types of curves as those in a for the Cl + CH_2FCl → CH_2F + Cl_2. **c** Same types of curves as those in a for the Cl + CH_2FCl → CH_2Cl + ClF

rapidly up to about $s = 0.42$ (amu)$^{1/2}$ bohr, and later, the changes become slow again. However, the lengths of the other bond show nearly no change during the entire reaction processes. The points where these remarkable changes take place indicate the beginning of the dissociation of the C–H bond [$s = -0.45$ (amu)$^{1/2}$ bohr] and the end of the formation of the H–Cl bond [$s = 0.42$ (amu)$^{1/2}$ bohr]. It is thus evident that hydrogen abstraction from C to Cl essentially takes place in the region of $s = -0.45$–0.42 (amu)$^{1/2}$ bohr. For $Cl + CH_2FCl \rightarrow CH_2F + Cl_2$ reaction channel (see Fig. 3b), the breaking C–Cl bond the forming Cl–Cl bond lengths change linearly along the reaction coordinate up to about $s = -0.05$ (amu)$^{1/2}$ bohr. From $s = -0.05$–0.05 (amu)$^{1/2}$ bohr both bonds change rapidly. After that, the breaking C–Cl bond length increases linearly again, and the forming Cl–Cl bond length decreases slowly until the reaction coordinate s reaches 0.70 (amu)$^{1/2}$ bohr and remains unchanged thereafter. This indicates that the beginning of the formation of the Cl–Cl bond is at $s = -0.05$ (amu)$^{1/2}$ bohr and the end of the formation of the Cl–Cl bond is at $s = 0.70$ (amu)$^{1/2}$ bohr. While the other bond lengths show nearly no change during the entire reaction processes. For the $Cl + CH_2FCl \rightarrow CH_2Cl + ClF$ reaction channel (see Fig. 3c), the bond length changes along the IRC are similar to the reaction channel $Cl + CH_2FCl \rightarrow CH_2F + Cl_2$. The different results between Fig. 3a and Fig. 3b or c are due to the structure of the transition state. For reaction R1, it proceeds via early barrier, while for reaction R2 and R3, they both proceed via late transition states.

The minimum-energy paths (MEPs) of the three reaction channels are calculated by the intrinsic reaction coordinate (IRC) theory at the MP2/6-311G(d, p) level. Using interpolated single-point energies (ISPE) approach, the potential profiles are further refined by four single-point calculations (ISPE-4) at QCISD(T)/6-311++G(d, p)//MP2/6-311G (d, p) level. Figure 4a–c depicts the classical potential energy curves $V_{MEP}(s)$ and the ground-state vibrational adiabatic potential energy curves $V_a^G(s)$ as functions of the intrinsic reaction coordinate s at QCISD(T)//MP2 level together with the zero-point energy curves ZPE(s), where $V_a^G(s) = V_{MEP}(s) + ZPE(s)$, for the three reaction channels. Table 2 lists the classical barrier height (V_{MEP}) and the vibrationally adiabatic ground state barrier height (V_a^G). In Fig. 4a, it can be seen that the curve of $V_a^G(s)$ is different in shape from the corresponding curve of $V_{MEP}(s)$. We can interestingly find that for H-abstraction reaction channel, the ground-state vibrational adiabatic potential surface $V_a^G(s)$ has a local maximum at $s = -0.45$ (amu)$^{1/2}$ bohr in the reactant side. The nonregular $V_a^G(s)$ shape may be attributed to the combination of two different factors: the low-energy

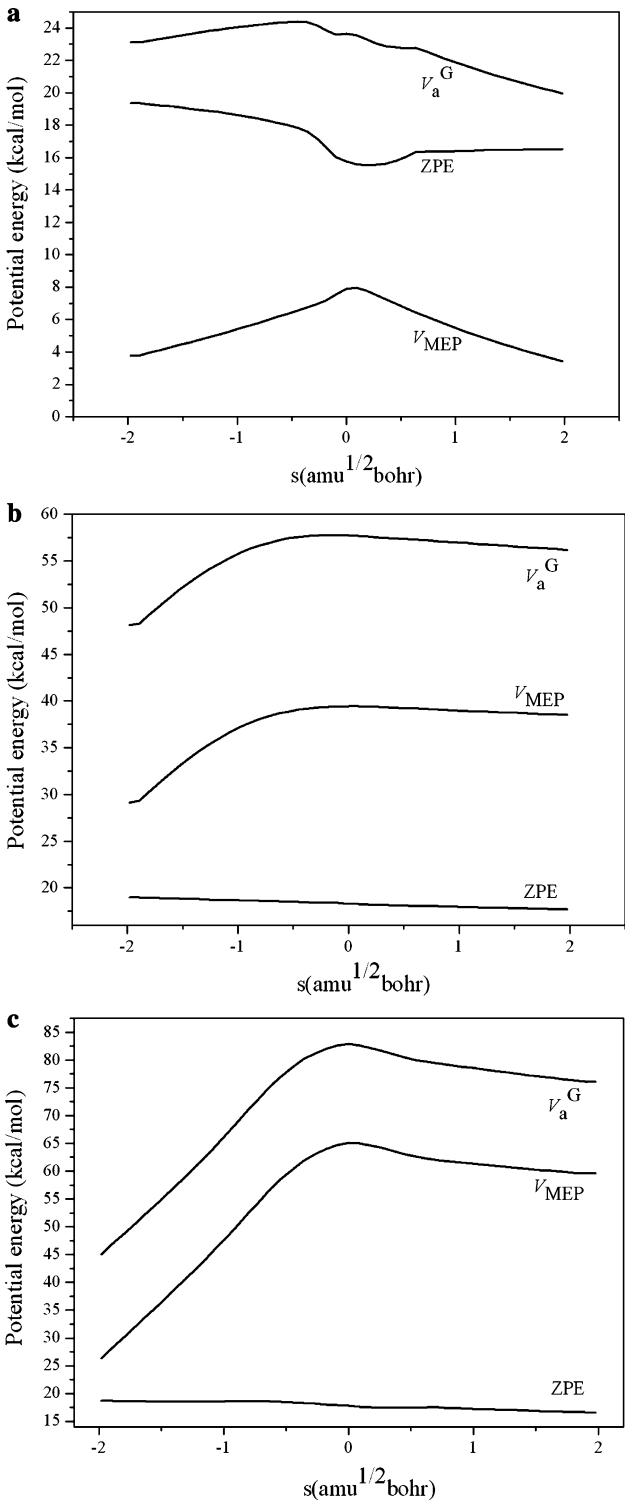

Fig. 4 **a** Classical potential energy ($V_{MEP}(s)$), zero-point energies (ZPE), and vibrational adiabatic potential energy ($V_a^G(s)$) as a function of the reaction coordinate, s, at the QCISD(T)//MP2 level for the $Cl + CH_2FCl \rightarrow CHFCl + HCl$. **b** Same types of curves as those in a for the $Cl + CH_2FCl \rightarrow CH_2F + Cl_2$. **c** Same types of curves as those in a for the $Cl + CH_2FCl \rightarrow CH_2Cl + ClF$

barrier and the relatively significant early drop in the zero-point energy (ZPE) curve prior to the saddle point zone [48]. This is not only a feature of the present reaction systems, but also has been observed in other reactions, as reported by Rosenman et al. [49] and Li et al. [50]. Since the curve of $V_a^G(s)$ differs obviously from the curve of $V_{MEP}(s)$ in shape, the variational effect might be very important in evaluating the rate constants. In order to understand variational effect further, the dynamics bottleneck property of the reaction R1 based on the canonical variational transition state approach are calculated. The dynamics bottleneck properties denote that the position s of the variational transition state at various temperatures deviates from the saddle point at $s = 0$. For the reaction channel R1 $Cl + CH_2FCl \rightarrow CHFCl + HCl$, the maximum value of shifted s is -0.04 $(amu)^{1/2}$ bohr at 220 K, where the values of $V_{MEP}(s = -0.04)$ and $V_a^G(s = -0.04)$ are 9.24 and 25.08 kcal/mol. The differences, $V_{MEP}(s = -0.04) - V_{MEP}(s = 0) = -0.028$ kcal/mol, and $V_a^G(s = -0.04) - V_a^G(s = 0) = 0.05$ kcal/mol, are small. It can, therefore, be concluded that the variational effect on the rate constant is small. For the remaining two reaction channels, i.e., (R2) $Cl + CH_2FCl \rightarrow CH_2F + Cl_2$ and (R3) $CH_2FCl \rightarrow CH_2Cl + ClF$ (see Fig. 4b, c), the $V_{MEP}(s)$ and $V_a^G(s)$ curves are similar in shape, and their maximum positions are almost the same. The zero-point energy ZPE curves are practically constants as s varies with only a gentle fall near the saddle point ($s = 0$). As a result, for the two reaction channels (R2 and R3), the variational effect on the calculation of rate constant will also be small, as will be confirmed by the rate constant calculations.

3.3 Rate constants

The rate constants of the individual channel, k_1, k_2, and k_3 are calculated by conventional transition state theory (TST), canonical variational transition state theory (CVT), and the CVT with the small-curvature tunneling (SCT) contributions in a wide temperature range from 220 to 3,000 K at the QCISD(T)/6-311++G(d, p)//MP2/6-311G(d, p) level of theory. The calculated rate constants of the three reaction channels are displayed in Table 3 and plotted against the reciprocal of temperature in Fig. 5a–c together with the corresponding experimental data. From Table 3 and Fig. 5a–c, we can see that for reaction R1, R2, and R3, the CVT rate constants and the TST rate constants are nearly the same over the whole temperature range 220–3,000 K. This means that the variational effect is small for the three reaction channels. For the reaction R1 and R3 channels, the tunneling effect, that is, the ratio between CVT/SCT and CVT rate constant, plays an important role in the calculation of rate constants at low temperatures and becomes negligible in the high temperature range. For example, the ratios of k_1(CVT/SCT)/k_1(CVT) are 1.71 at 220, 1.35 at 300, 1.19 at 400, 1.08 at 600, 1.03 at 1,000, and 0.99 at 3,000 K, respectively. The ratios of k_3(CVT/SCT)/k_3(CVT) are 96.10, 10.10, 3.42, 2.15, 1.25, 1.05, and 1.02 at 220, 300, 400, 500, 800, 2,000, and 3,000 K, respectively. For the reaction R2 channel, Fig. 5b shows that the CVT and CVT/SCT rate constants are nearly the same over the whole temperature range 220–3,000 K, and this means that the tunneling effect is small.

Table 3 The calculated CVT/SCT rate constants [$(cm^3/(molecule\ s)]$ of three reaction channels and the overall rate constants k [$cm^3/(molecule\ s)$] in the temperature range 220–3,000 K

T (K)	k_1	k_2	k_3	k
220	3.12E−14	4.94E−42	8.10E−73	3.12E−14
230	3.84E−14	1.05E−40	2.94E−70	3.84E−14
250	5.60E−14	2.28E−38	1.00E−65	5.60E−14
298	1.19E−13	5.24E−34	3.13E−57	1.19E−13
300	1.22E−13	7.44E−34	6.22E−57	1.22E−13
330	1.80E−13	8.64E−32	6.92E−53	1.80E−13
400	3.78E−13	3.76E−28	1.01E−45	3.78E−13
500	8.47E−13	1.11E−24	7.34E−39	8.47E−13
600	1.58E−12	2.46E−22	3.19E−34	1.58E−12
700	2.62E−12	1.22E−20	7.15E−31	2.62E−12
900	5.74E−12	2.40E−18	2.39E−26	5.74E−12
1,000	7.90E−12	1.57E−17	9.58E−25	7.90E−12
1,200	1.32E−11	2.74E−16	2.55E−22	1.32E−11
1,400	2.02E−11	2.19E−15	1.45E−20	2.02E−11
1,500	2.43E−11	5.09E−15	7.37E−20	2.43E−11
1,700	3.38E−11	2.07E−14	1.10E−18	3.38E−11
2,000	5.10E−11	1.04E−13	2.39E−17	5.11E−11
2,200	6.45E−11	2.43E−13	1.19E−16	6.47E−11
2,400	7.95E−11	5.00E−13	4.57E−16	8.00E−11
2,600	9.60E−11	9.27E−13	1.45E−15	9.69E−11
3,000	1.33E−10	2.55E−12	9.35E−15	1.36E−10

The CVT/SCT rate constants of k_1 at 298 K, 1.19×10^{-13} $cm^3/(molecule\ s)$, are in good agreement with the available experimental value of $(1.1 \pm 0.25) \times 10^{-13}$ $cm^3/(molecule\ s)$ [18]. The overall theoretical CVT/SCT rate constants k for the title reaction are calculated from the sum of the corresponding individual rate constants, that is, $k = k_1 + k_2 + k_3$. The deviation between the theoretical and experimental values remains within a factor of approximately 1.06. Thus, the present calculations may provide reliable prediction of the rate constants for the title reaction over a wide temperature range.

Table 3 shows that the rate constants of reaction R1, k_1, are about 27-2 and 58-6 orders of magnitude higher than those of the rate constants of k_2 and k_3, from 220 to 2,000 K, respectively. Thus, we can conclude that the H-abstraction channel, reaction R1, is always absolute

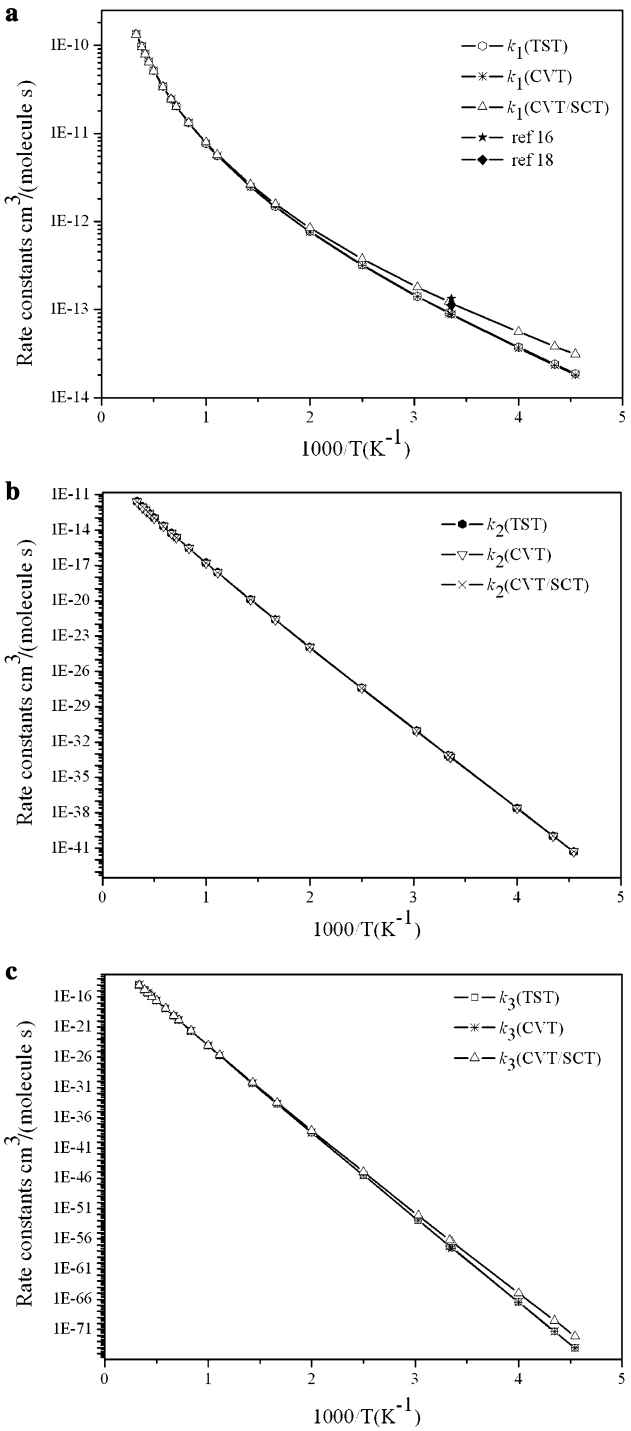

Fig. 5 The TST, CVT, and CVT/SCT rate constants as a function of $10^3/T$ between 220 and 3,000 K for the **a** $Cl + CH_2FCl \rightarrow CHFCl + HCl$. **b** $Cl + CH_2FCl \rightarrow CH_2F + Cl_2$. **c** $Cl + CH_2FCl \rightarrow CH_2Cl + ClF$, together with the available experimental values

dominant in the temperature of 220–2,000 K and reactions R2 and R3 are minor pathways. It is consistent with the analysis result from the potential barrier heights of these three reaction channels. The contribution of k_2 and k_3 to the overall rate constants increases as the temperature increases, while reaction R2 becomes more and more competitive with the temperature increase from 2,000 to 3,000 K.

Finally, for convenience of future experimental measurements, we give three-parameter rate constant expressions by fitting the theoretical results for the three reaction channels and the whole reaction in the temperature range of 220–3,000 K, and the expressions are given as follows: [in unit of $cm^3/(molecule\ s)$]

$$k_1(T) = 4.79 \times 10^{-17} T^{1.90} \exp(-1128.81/T),$$

$$k_2(T) = 3.11 \times 10^{-15} T^{1.48} \exp(-15579.36/T),$$

$$k_3(T) = 2.08 \times 10^{-14} T^{1.26} \exp(-32813.08/T),$$

$$k(T) = 1.48 \times 10^{-17} T^{2.04} \exp(-913.91/T).$$

4 Conclusion

In this paper, the reaction $Cl + CH_2FCl \rightarrow$ products have been studied by dual-level direct dynamics methods. The potential energy surface information is obtained at the MP2/6-311G(d, p) level, and higher-level energies are improved at the QCISD(T)/6-311++G(d, p) level. Three reaction channels are identified, i.e. H-abstraction, Cl-abstraction, and F-abstraction. The calculated potential barriers show that the major pathway is H-abstraction channel leading to the products, CHFCl + HCl. For each individual reaction channel, the theoretical rate constants in the temperature region of 220–3,000 K are calculated by the canonical variational transition state theory (CVT) with the small-curvature tunneling correction (SCT). The calculated total rate constants of these reactions are in good agreement with the corresponding experimental values. The results show that H-abstraction channel is important at lower temperatures; the Cl-abstraction should be considered when the temperature is higher the 2,000 K. The F-abstraction reaction channel is a minor channel over the whole temperature region. The rate constant calculations show that the overall rate constants have positive temperature dependence. It is found that the variational effect is small for the three reaction channels. The small-curvature tunneling effect plays an important role at the lower temperatures for reaction channels R1 and R3, while it is small for the reaction channel R2. Our results may be useful for further experimental studies on the dynamical properties of the title reaction.

Acknowledgments The authors thank Prof. Donald G. Truhlar for providing POLYRATE 9.1 program. This work is supported by the National Natural Science Foundation of China (No. 20773021), and Training Fund of NENU'S Scientific Innovation Project (NENUSTC07016). We are greatly thankful for the referees' helpful comments.

References

1. Tuck R, Plumb A, Condon E (1990) Geophys Res Lett 17:313. doi:10.1029/GL017i004p00313
2. Rosswall T (1991) Environ Sci Technol 25:567. doi:10.1021/es00016a001
3. Atkinson R (1986) Chem Rev 86:69. doi:10.1021/cr00071a004
4. Atkinson R (1994) J Phys Chem Ref Data Monograph 2:1–216
5. Manzer L (1990) Science 249:31. doi:10.1126/science.249.4964.31
6. Manning RG, Kurylo MJ (1977) J Phys Chem 81:291. doi:10.1021/j100519a003
7. Senkan SM (1988) Environ Sci Technol 22:368. doi:10.1021/es00169a600
8. Bryukov MG, Slagle IR, Knyazev VD (2001) J Phys Chem A 105:6900. doi:10.1021/jp0106505
9. Zhang H, Zhang GL, Wang L, Liu B, Yu XY, Li ZS (2006) Chem Phys Lett 432:6. doi:10.1016/j.cplett.2006.10.024
10. Knyazev VD (2003) J Phys Chem A 107:11082. doi:10.1021/jp036281p
11. Li S, Li ZS, Liu JY, Sun CC (2004) J Comput Chem 25:72. doi:10.1002/jcc.10305
12. Li QS, Wang CY (2002) Phys Chem Chem Phys 4:4386. doi:10.1039/b206133n
13. Sun H, He HQ, Pan YR, Pan XM, Li ZS, Wang RS (2008) Chem Phys Lett 450:186. doi:10.1016/j.cplett.2007.11.003
14. Zhang H, Wu JY, Li ZS, Liu JY, Li S, Sun CC (2005) J Comput Chem 26:1421. doi:10.1002/jcc.20283
15. Wang L, Liu JY, Wan SQ, Li ZS (2008) Chem Phys Lett 455:20. doi:10.1016/j.cplett.2008.02.006
16. Tschuikow-Roux E, Faraji F, Paddison S, Niedzielski J, Miyokawa K (1988) J Phys Chem 92:1488. doi:10.1021/j100317a023
17. Jourdain GL, Poulet G, Barassin J, LeBras G, Combourieu J (1977) J Pollut Atmos 75:256
18. Tuazon EC, Atkinson R, Corchnoy SB (1992) Int J Chem Kinet 24:639. doi:10.1002/kin.550240704
19. Senkan SM, Quam D (1992) J Phys Chem 96:10837. doi:10.1021/j100205a044
20. Wallington TJ, Hurley MD, Schneider WF, Sehested J, Nielsen OJ (1994) Chem Phys Lett 218:34. doi:10.1016/0009-2614(93)E1466-T
21. Atkinson R, Baulch DL, Cox RA et al (1997) J Phys Chem Ref Data 26:521
22. Bell RL, Truong TN (1994) J Chem Phys 101:10442. doi:10.1063/1.467862
23. Truong TN, Duncan WT, Bell RL (1996) In: Chemical applications of density functional theory. American Chemical Society, Washington, DC, p 85
24. Truhlar DG (1995) In: Heidrich D (ed) The reaction path in chemistry: current approaches and perspectives. Kluwer, Dordrecht, p 229
25. Corchado JC, Espinosa-Garcia J, Hu WP, Rossi I, Truhlar DG (1995) J Phys Chem 99:687. doi:10.1021/j100002a037
26. Hu WP, Truhlar DG (1996) J Am Chem Soc 118:860. doi:10.1021/ja952464g
27. Truhlar DG, Garrett BC (1980) Acc Chem Res 13:440. doi:10.1021/ar50156a002
28. Truhlar DG, Isaacson AD, Garrett BC (1985) In: Baer M (ed) The theory of chemical reaction dynamics, vol 4. CRC Press, Boca Raton, p 65
29. Frisch MJ, Trucks GW, Schlegel HB et al (2004) Gaussian 03, revision C.02. Gaussian, Inc., Wallingford
30. Duncan WT, Truong TN (1995) J Chem Phys 103:9642. doi:10.1063/1.470731
31. Gonzalez C, Schlegel HB (1989) J Chem Phys 90:2154. doi:10.1063/1.456010
32. Corchado JC, Chuang YY, Fast PL et al (2002) POLYRATE version 9.1. Department of Chemistry and Supercomputer Institute, University of Minnesota, Minneapolis, MN
33. Chuang YY, Corchado JC, Truhlar DG (1990) J Phys Chem A 103:1140. doi:10.1021/jp9842493
34. Garrett BC, Truhlar DG (1979) J Chem Phys 70:1593. doi:10.1063/1.437698
35. Garrett BC, Truhlar DG (1979) J Am Chem Soc 101:4534. doi:10.1021/ja00510a019
36. Garrett BC, Truhlar DG, Grev RS, Magnuson AW (1980) J Phys Chem 84:1730. doi:10.1021/j100450a013
37. Truhlar DG, Issacson AD, Skodje RT, Garrett BC (1983) J Phys Chem 87:4554. doi:10.1021/j100245a604
38. Lu DH et al (1992) Comput Phys Commun 71:235. doi:10.1016/0010-4655(92)90012-N
39. Liu YP, Lynch GC, Truong TN, Lu DH, Truhlar DG, Garrett BC (1993) J Am Chem Soc 115:2408. doi:10.1021/ja00059a041
40. Lide DR (1999) In: CRC Handbook of chemistry and physics, 80th edn. CRC Press, Boca Raton
41. Huber KP, Herzberg G (1979) In: Molecular spectra and molecular structure IV. Constants of diatomic molecules. Van Nostrand Reinhold Co., New York
42. Harmony MP, Laurie VW, Ramsay RL, Lovas FJ, Lafferty WJ et al (1979) J Phys Chem Ref Data 8:619
43. Chase MW Jr, Davies CA, Downey JR, Fryrip DJ, McDonald RA, Syverud AN JANAF (1985) Thermochemical tables, Suppl 1, vol 14, 3rd edn, Ref Data, pp 1–926
44. NIST Chemistry WebBook (2005) NIST Standard Reference Database Number 69, June Release (vibrational frequency data compiled by Jacox ME)
45. NIST Chemistry WebBook (2003) NIST Standard Reference Database Number 69, March Release (date compiled by Huber KP and Herzberg G)
46. Chase MW Jr (1998) Thermochemical tables NIST-JANAF, 4th edn. J Phys Chem Ref Data, Monograph 9, Suppl 1
47. Tschuikow-Roux E, Paddison S (1987) Int J Chem Kinet 19:15. doi:10.1002/kin.550190103
48. Poutsma JC, Paulino JA, Squires RR (1997) J Phys Chem A 101:5327. doi:10.1021/jp970778f
49. Rosenman E, McKee ML (1997) J Am Chem Soc 119:9033. doi:10.1021/ja9711851
50. Xiao JF, Li ZS, Ding YH et al (2002) J Phys Chem A 106:320. doi:10.1021/jp013405u